
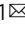





Arctic open-water periods are projected to lengthen dramatically by 2100

Alex Crawford ¹, Julienne Stroeve^{1,2,3}, Abigail Smith ⁴ & Alexandra Jahn ⁴

The shrinking of Arctic-wide September sea ice extent is often cited as an indicator of modern climate change; however, the timing of seasonal sea ice retreat/advance and the length of the open-water period are often more relevant to stakeholders working at regional and local scales. Here we highlight changes in regional open-water periods at multiple warming thresholds. We show that, in the latest generation of models from the Coupled Model Intercomparison Project (CMIP6), the open-water period lengthens by 63 days on average with 2 °C of global warming above the 1850-1900 average, and by over 90 days in several Arctic seas. Nearly the entire Arctic, including the Transpolar Sea Route, has at least 3 months of open water per year with 3.5 °C warming, and at least 6 months with 5 °C warming. Model bias compared to satellite data suggests that even such dramatic projections may be conservative.

¹Centre for Earth Observation Science, University of Manitoba, Winnipeg, MB, Canada. ²Department of Earth Sciences, University College London, London, UK. ³National Snow and Ice Data Center, Cooperative Institute for Research in Environmental Science, University of Colorado, Boulder, CO, USA. ⁴Department of Atmospheric and Oceanic Sciences and Institute of Arctic and Alpine Research, University of Colorado, Boulder, CO, USA. email: alex.crawford@umanitoba.ca

Rapid decline of Arctic sea ice extent in the late twentieth century was an early signal that anthropogenic climate change was not just a future likelihood but a present reality^{1,2}. Exceptional decreases have continued in both sea ice extent^{3,4} and thickness⁵, and model projections of the future suggest frequent ice-free Septembers with 2 °C of warming from pre-industrial conditions^{6–8}, or by the middle of the twenty-first century^{9–12}. Ice-free Septembers are less likely but still possible even under a 1.5 °C warming scenario^{7,8,11}. Pan-Arctic September sea ice extent is a useful long-term climate indicator; however, regional variability is large¹⁰, and regional and local sea ice conditions are often most relevant for specific stakeholders in the Arctic^{13–15}. At these scales, the length of the seasonal open-water period has major implications for phytoplankton productivity^{16,17}, coastal erosion¹⁸, hunting and fishing^{13,19}, marine shipping^{14,15}, and tourism²⁰. The timing of sea ice retreat and advance, more particularly, also have important implications. For example, the most intense Arctic storms occur November to February²¹, so delayed sea ice advance exacerbates ocean swell¹⁸.

Since 1979, the open-water period has increased in nearly every region of the Arctic Ocean, due both to earlier retreat and later advance^{22–25}. In the Pacific-side Arctic, the trend toward later advance outpaces the trend toward earlier retreat^{25–27}. The larger change in ice advance is a result of more ocean heat-uptake in summer as a result of earlier formation of open water, which in turn delays fall advance^{28–30}. However, in other regions (e.g., Hudson Bay) the trend toward earlier retreat day drives observed lengthening of the open-water period²⁵.

A few studies have examined future projections of open-water periods using a previous intercomparison of global climate models (CMIP5), but only under a high-emissions scenario (RCP8.5). These simulations show that the lengthening of the projected pan-Arctic open-water period through 2200 is dominated by later ice advance³⁰. Under RCP8.5 in one CMIP5 model (the Community Earth System Model), the open-water period exceeds 6 months a year by 2100 throughout most of the Arctic Ocean, including the Transpolar Sea Route³¹. However, the impacts of warming lower than projected under RCP8.5 (i.e., below 4 °C³²) have not been assessed, although they are highly relevant given the Paris Agreement goal of limiting warming to less than 2 °C³³, which is much less than achieved under RCP8.5 by 2100 (Supplementary Fig. 1). To address this gap, we here provide stakeholder relevant projections of open-water periods for 15 Arctic regions as well as the Northern Sea Route and the Transpolar Sea Route. The open-water period is assessed in terms of both time and global temperature anomalies (e.g., 1.5 and 2 °C) using output from CMIP6 models forced by low, medium and high emissions scenarios (SSP126, SSP245, and SSP585). This assessment aims to provide guidance and future projections of the open-water period (and the timing of sea ice retreat and advance) at multiple spatial scales and temperature thresholds. If and when we reach those thresholds depends on the choices that we make today.

Results

Comparison of CMIP6 models to satellite record. For this study, sea ice retreat day is defined as the last time sea ice concentration (SIC) falls below 15% before reaching its minimum annual value. Advance day is the first time after the minimum that SIC rises above 15%. The time between retreat and advance is the open-water period.²⁴ To assess the robustness of future projections of the open-water period, we first evaluate how well CMIP6 models capture its historical average, trend, and sensitivity to temperature. The pan-Arctic multi-model mean of the average open-water period is nearly identical to the observational

mean (Fig. 1a). However, several models underestimate the length of the open-water period, indicated by lying beyond the X's that mark the uncertainty range around the observational mean. This range is calculated by combining the average internal variability in the models with the uncertainty in the observations (Eqs. 1–4). Internal variability for each of the 19 models with at least three simulations is plotted as gray shading centered on the observational mean.

Examining each region, underestimation of the open-water period is most prevalent in the Greenland and Barents seas, which have long open-water periods and together comprise 20% of the study area. By contrast, overestimation is more common in the Gulf of St. Lawrence, Canadian Arctic Archipelago, Beaufort Sea, Chukchi Sea, Kara Sea, and Hudson Bay (34% of the study area altogether). This is consistent with Smith et al.³⁴, who reported mean open-water periods were overestimated for the area north of 66°N in a subset of CMIP6 models. Altogether, a good match exists between models and observations for the pan-Arctic mean, but this occurs in part because of compensating biases in different regions, highlighting the importance of regional analysis.

Figure 1d shows what percentage of each region is open before the first day of the given month. The later the average retreat day is in a region, the smaller the percentage will be. This metric is better than using the average retreat day because the retreat day is an invalid quantity if SIC is always above or always below 15% for the entire year. Especially with climate change, the size of the area in each region that has valid retreat days each year changes, which can mask trends. Taking the percentage of each region open before a given date avoids this issue. If sea ice retreat is biased early in a model, the retreat percentage will be overestimated, and the model will lie above the uncertainty range. If sea ice retreat is biased late, the retreat percentage will be underestimated.

In general agreement with previous analysis³⁴, bias resulting in excessively long open-water periods always occurs because of sea ice retreat occurring too early in the multi-model mean, and sometimes also advance occurring too late (Fig. 1d–e). Specifically, Hudson Bay, the Gulf of St. Lawrence, and the Beaufort Sea exhibit both biases; the Kara Sea and Canadian Arctic Archipelago only exhibit too early retreat. The only case of sea ice retreat occurring too late is in the Sea of Okhotsk. This partially compensates for the bias in other regions, so pan-Arctic retreat shows less consistent bias than the area poleward of 66°N described by Smith et al.³⁴ No region exhibits a multi-model mean biased toward too early advance.

The historical trend (1979–2013) in open-water period (Fig. 1b) and the sensitivity of open-water period to pan-Arctic temperature anomalies (Fig. 1c) show substantial internal variability in model ensembles, making the uncertainty range around the observations relatively large. Therefore, although the trend and temperature sensitivity are higher for observations than the multi-model mean in nearly every region (the Bering Sea being a notable exception), the multi-model mean is within the observational uncertainty range for all regions. In other words, discrepancies between models and observations could be explained by internal variability. However, especially for temperature sensitivity, there are many more cases of models falling below the uncertainty range than above, suggesting that the open-water period in some CMIP6 models may not be sensitive enough to warming.

The multi-model mean of the metrics used for regional retreat and advance of sea ice similarly show stronger trends and temperature sensitivity for observations than for the multi-model mean (Fig. 1f–i). In several regions, this discrepancy cannot be explained by internal variability. Sensitivity to pan-Arctic warming is too low in the multi-model mean for both retreat and advance in the Laptev Sea. For Hudson Bay and the Chukchi,

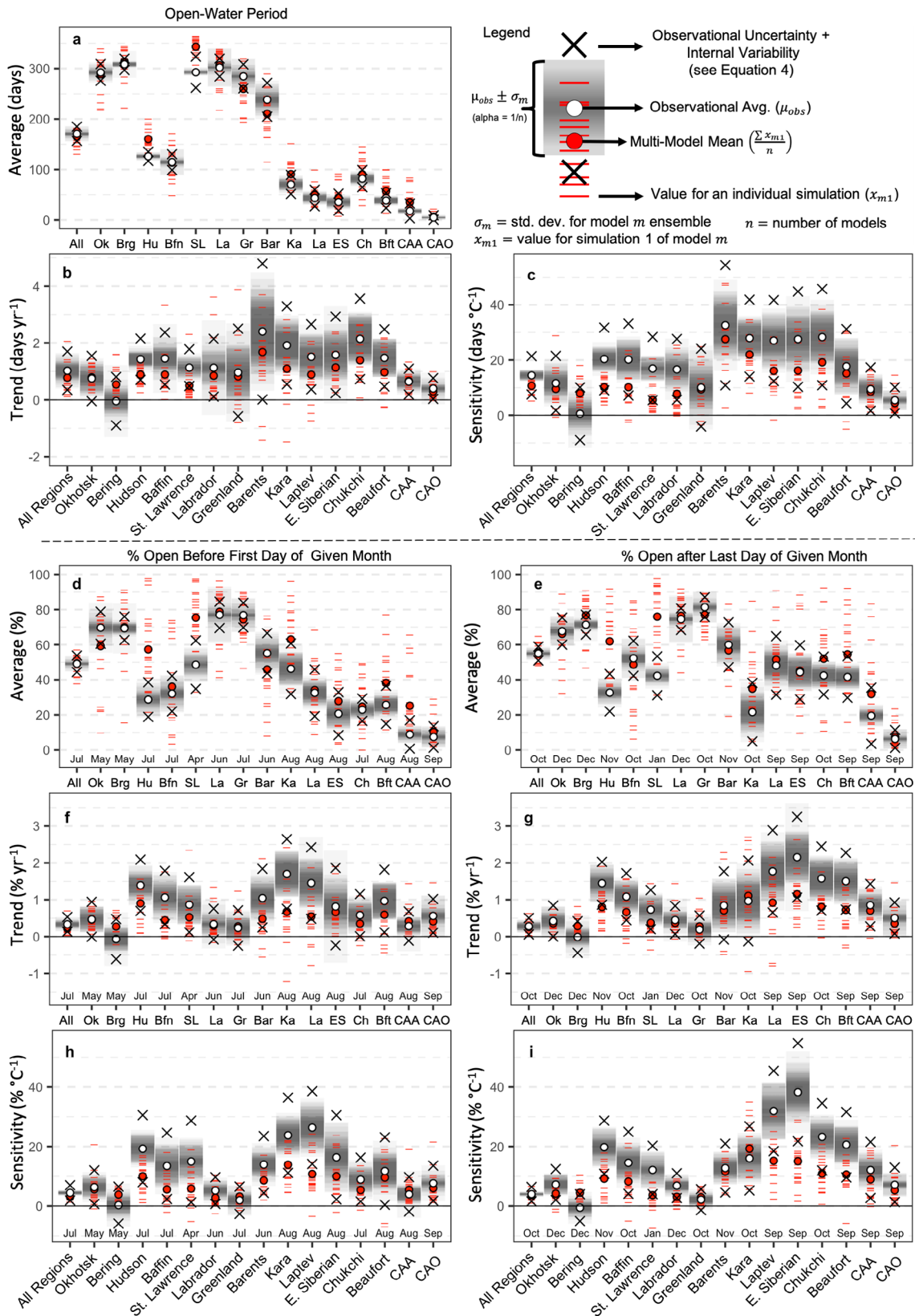


Fig. 1 Regional comparison of CMIP6 models and observations. Averages, trends, and sensitivity to pan-Arctic temperature (latitude $\geq 60^\circ\text{N}$) are calculated for **a-c** open-water period, **d, f, h** the percent of regional area with permanent open water or sea ice retreat before the first of the given month, and **e, g, i** the percent of the regional area with permanent open water or sea ice advance after the last day of the given month (more details in “Methods” section). All calculations are for the overlap period between the historical CMIP6 experiments and the satellite record (1979–2013). The multi-model mean (red dot) is the average of the first simulation for each of 21 models. The gray shading around each observational mean (μ_{obs} ; white dots) is produced by plotting $\mu_{obs} \pm \sigma_m$, where σ_m is the standard deviation of the model’s ensemble for each of 19 models with an ensemble of at least three simulations. The opacity is set to 1/19, so the darker the shading at a given value, the more models agree that this value is within the range of internal variability. CAO Central Arctic Ocean, CAA Canadian Arctic Archipelago.

East Siberian, and Beaufort seas, sensitivity to pan-Arctic warming is only too low for sea ice advance. Overall, more bias exists in the temperature sensitivity than in the trends, which is consistent with how some models that overestimate warming better match the observed trend in September sea ice extent^{35,36}. Because there are no compensating biases in other regions (i.e., nowhere is the sensitivity to pan-Arctic warming overestimated by the multi-model mean), low sensitivity is more likely caused by a bias in energy transfer between the atmosphere and ice/ocean surface than a bias in dynamics.

Because of the positive feedback between SIC, albedo, and ocean heat-uptake, earlier ice retreat is typically followed by later ice advance²⁴. Past studies have found that this feedback amplifies the trend toward later advance, leading to a stronger change in advance day than retreat day in observations^{24,26} and CMIP5 models^{27,30}. It would be logical, then, if the temperature sensitivity of sea ice advance in Hudson Bay and the Chukchi, East Siberian, and Beaufort seas stemmed from these positive feedbacks being too weak. However, compared to observations, CMIP6 models yield similar or stronger correlations between de-trended sea ice retreat day and advance day (1979–2013; Supplementary Fig. 2), consistent with a strong ice-albedo feedback. The four regions in question are no exception.

These results have focused on an open-water period defined by retreat and advance relative to 15% SIC. Using 80% as the SIC threshold yields longer open-water periods, but results are otherwise comparable to using a 15% SIC threshold for most regions (Supplementary Figs. 3–6). Hudson Bay is the clear exception. Although the open-water period is too long for Hudson Bay in nearly every model when using 15% (Fig. 1a), the multi-model mean is well within the observational uncertainty range using 80% (Supplementary Fig. 3). In other words, for several models, opening in Hudson Bay begins at a reasonable time, but the ice-loss period is too rapid.

Projections of future open-water period. The rate of increase in open-water period is comparable for all three emissions scenarios until the 2040s (Fig. 2), when the rate of change declines in SSP126 (blue), persists in SSP245 (orange), and accelerates in SSP585 (red). The most southerly regions (Sea of Okhotsk, Bering Sea, Gulf of St. Lawrence, and Labrador Sea) become ice-free year-round by the end of the century in SSP585, and some models also show the Greenland and Barents seas reach 365 days of open water for all grid cells by 2100. Winter sea ice still forms in all regions except the Gulf of St. Lawrence in SSP126. The absence of sea ice in this region for SSP126 may not be credible, though, since the multi-model mean open-water period is biased high for 1979–2013.

The Kara, Laptev, East Siberian, Chukchi, and Beaufort seas all experience dramatic ice cover changes from 1950 to 2100: going from about 2–3 months to 9–10 months of open water in SSP585. Changes in SSP126 are much less dramatic: up to 4–5 months in the Kara, Laptev, and East Siberian Seas and 6 months in the Chukchi and Beaufort Seas by 2100. At least for the Chukchi Sea, this represents faster change in CMIP6 than CMIP5. The mean SSP585 trend for the Chukchi Sea is $+1.66 \pm 0.22$ days yr^{-1} from 2015 to 2044, which is about twice as fast as in the subset of CMIP5 models used by Wang et al.²⁷ under the similar RCP8.5 scenario. Another area undergoing dramatic changes is the central Arctic Ocean, which had mostly perennial ice cover in the historical experiments, but by 2100, has up to 3 months (SSP126) or nearly 8 months (SSP585) of open-water conditions on average. The open-water period in Hudson Bay extends to over 10 months per year by 2100 under SSP585. Since the multi-model mean overestimates Hudson Bay open-water periods by

about a month (34 days; Fig. 1a), a more realistic estimate may be exceeding 9 months by 2100. However, since Hudson Bay exhibits a better match between CMIP6 models and observations using 80% SIC instead of 15% (Supplemental Fig. 3a), the 11-month open-water period below 80% SIC by 2100 under SSP585 (Supplemental Fig. 4c) is likely reasonable.

Trends in open-water period incur errors both from errors in sensitivity of open-water period to warming and errors in sensitivity of temperature to emissions. Comparing the length of the open-water period to global temperature anomalies of 0 and 2 °C relative to 1850–1900 (Fig. 3a) eliminates the error source related to the sensitivity of temperature to emissions and is independent of emissions scenario (Supplementary Fig. 7). Additionally, average global warming by 2100 in the aggressive emission-reduction scenario (SSP126) for these models is exactly 2.0 °C. With 2 °C of warming, the open-water period increases on average by about 2 months (63 days) overall, with the greatest changes in the Barents (123 days), Chukchi (99), Kara (99), and East Siberian (92) seas. With about half of the 2 °C of warming having occurred by 2013, it is unsurprising that these are also the fastest-changing seas during the satellite record. From 1979 to 2016, the Barents Sea was the greatest contributor to sea ice area loss in every month from November through March, and the Kara, Chukchi, and East Siberian seas were the three greatest contributors to September sea ice loss⁴. Major change is also apparent in the central Arctic Ocean. This region exhibits a relatively moderate increase in open-water period (56 days), but that is compared to nearly ubiquitous permanent ice cover in the late twentieth century.

The increase in open-water period results from both earlier sea ice retreat (Fig. 3b) and later sea ice advance (Fig. 3c). Overall, the percentage of grid cells experiencing retreat before July 1 goes from 44 to 61%, and the percentage experiencing advance after October 31 goes from 49 to 74%. Greater change in advance than retreat is consistent with observations^{24,26}, CMIP5 (refs. ^{27,30,31}), and our understanding of the ice-albedo feedback^{22,24,37}. The greatest amplification of changing advance compared to changing retreat in CMIP6 is in the Kara and Chukchi seas (Supplementary Fig. 8). Based on observed trends, these two seas have been projected as the most likely to transition to having permanent open water areas next (after the Barents Sea)⁴.

Maps of the year or temperature threshold at which the open-water period will exceed 90, 180, or 270 days (Fig. 4) highlight how continued warming will increase accessibility of shipping routes crossing multiple regions. The Northern Sea Route has two choke points (at Severnaya Zemlya and the New Siberian Islands) that open for over 90 days on average above 3.0 °C of warming from 1850–1900 levels. With 3.5 °C of warming, almost all of the Arctic Ocean (and therefore the Transpolar Sea Route) has a 90-day open-water period (Fig. 4j), with only parts of the Canadian Arctic Archipelago and north of Greenland being open for less time. When this occurs consistently (at least 5 years in a row) depends strongly on the emissions scenario: by 2070 in SSP585, by 2090 in SSP245, and not at all before 2100 in SSP126. This is comparable to past work showing ice-free conditions (average SIC < 15%) for August–October in the central Arctic Ocean by the 2050s in the multi-model mean under SSP585 but stabilizing with no ice-free conditions before 2100 in SSP126 (ref. ¹⁰).

The CMIP6 multi-mean shows 2085 as the first year that the average open-water period north of 80°N regularly exceeds 180 days under the SSP585 scenario. This is similar to results from the Community Earth System Model³⁸ under the RCP8.5 scenario, for which the central Arctic Ocean is open for over 180 days by 2100 (ref. ³¹). Here we show that this occurs only with 5.0 °C of warming (Fig. 4k), and so is avoided in the twenty-first century with SSP245 or SSP126. In the CMIP6

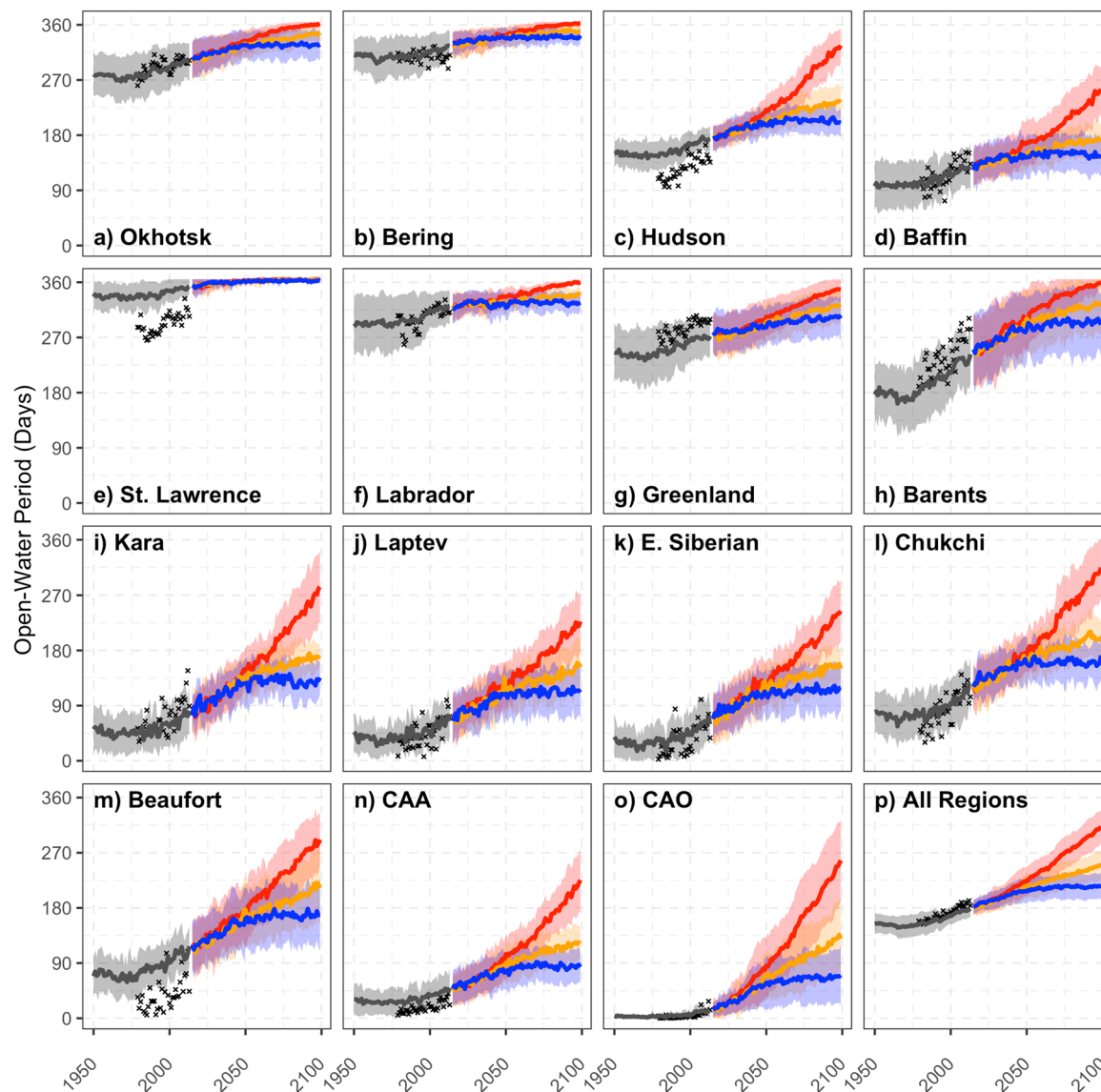


Fig. 2 Timeseries of regional open-water period. Open-water period is averaged for 15 Arctic sea ice regions (a–o) and the pan-Arctic (p). Timeseries include mean satellite observations (black xs) and CMIP6 experiments: historical (gray; $n = 21$), SSP585 (red; $n = 20$), SSP245 (orange; $n = 20$), and SSP126 (blue; $n = 19$). CMIP6 data are depicted as the multi-model means (solid lines) ± 1 standard deviation (shading). Only the first simulation from each model is used. CAO Central Arctic Ocean, CAA Canadian Arctic Archipelago.

models, open-water periods exceed 270 days for the Bering Sea, most of Hudson Bay, and even part of the Kara Sea at 4.5 °C of warming. The entire Chukchi Sea becomes open for at least 270 days with 5.5 °C. However, even under the strongest warming scenario, places like Baffin Bay, the Laptev Sea, and the Beaufort Sea maintain over 3 months of sea ice cover beyond 2100 (Fig. 4i). Under SSP126, those same regions still have sea ice for over half the year in 2100 (Fig. 4b). This is consistent with using monthly SIC instead of the open-water period¹⁰.

Discussion and conclusions

CMIP6 models exhibit some bias in the average open-water period in a few regions; for example, models exhibit an open-water period that is generally too long in Hudson Bay and too short in the Barents Sea. Because these biases roughly cancel out, they are obscured in the pan-Arctic average, which is more consistent with observations. The temperature sensitivity of the open-water period is higher in observations than the multi-model

mean for most regions (but not the Bering Sea). However, this can largely be explained by internal variability for many models. This is similar to results for pan-Arctic sea ice extent and area^{6,11,39} and regional monthly SIC¹⁰. Since there are no simulations for which the average or temperature sensitivity of open-water period falls within the uncertainty range for every region (Supplementary Fig. 9), no attempt was made here to examine a subset of high-performing models.

The CMIP6 multi-model mean matches several important characteristics of the historical open-water period and its response to warming. CMIP6 models correctly show rapid lengthening of the open-water period overall, especially in the Barents Sea (Fig. 1)^{22,24,25}. On the Pacific-side of the Arctic Ocean, lengthening has been driven more by later advance than by earlier retreat^{24–26}. The ice-albedo/ocean heat-uptake feedback in CMIP6 models is significantly stronger than in observations for some regions (Supplementary Fig. 2), and the CMIP6 multi-model mean captures the greater importance of the later advance in driving longer open-water periods (Fig. 1). However,

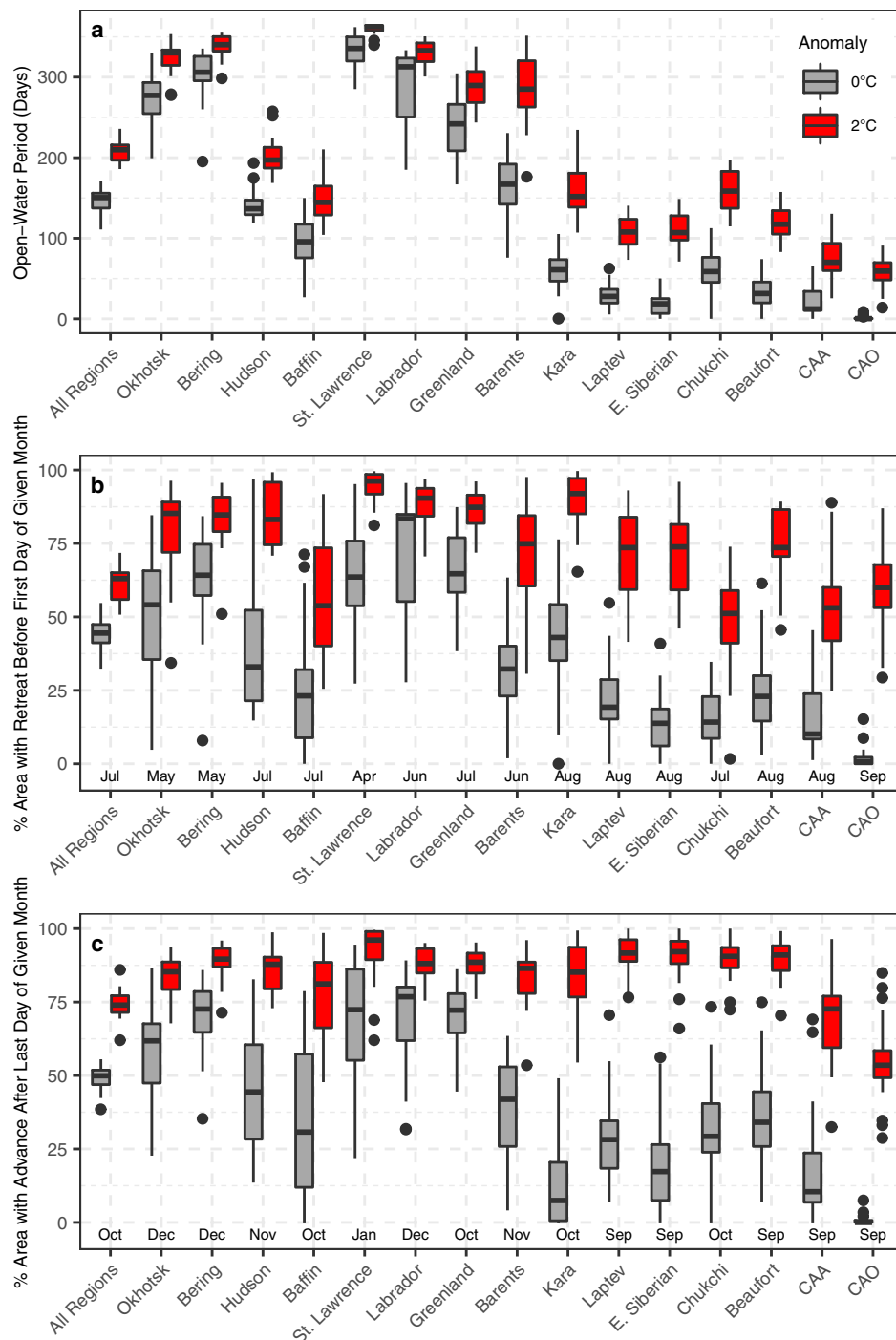


Fig. 3 Open-water period at 2°C global warming. Difference in regional open-water period (a), sea-ice retreat (b), and sea ice advance (c), for global temperature anomalies of 0°C (historical experiments) and 2°C (SSP585) relative to average global temperature for 1850–1900. Units for retreat are the percent of regional area with permanent open water or sea ice retreat before the first of the given month. Units for advance are the percent of the regional area with permanent open water or sea ice advance after the last day of the given month (more details in “Methods” section). Boxes represent the interquartile range of the first simulation for each of the 19 models with data for both historical and SSP585 simulations. Central lines indicate the median. Whiskers extend to the lowest and highest points that are within 1.5 times the interquartile range, and dots denote outliers. Each pair of medians is significantly different ($p < 0.05$) using a Wilcoxon signed-rank test.

temperature sensitivity for sea ice advance is too low in Hudson Bay and several Pacific-side seas, even accounting for the uncertainty from internal variability and satellite retrieval. In other words, the CMIP6 multi-model mean of the open-water period is generally a good match for observations, and the biases that exist may lead to conservative projections of sea ice change for the future.

Similar to what has been seen in CMIP5 models^{27,30,31}, the open-water period continues a steady lengthening and becomes months longer during the twenty-first century (Fig. 2), although CMIP6 models show faster change than CMIP5 in some areas (e.g., the Chukchi Sea). Continuing the observed change over the historical period^{25–27}, and similar to projections from the Community Earth System Model Large Ensemble³¹, CMIP6 models

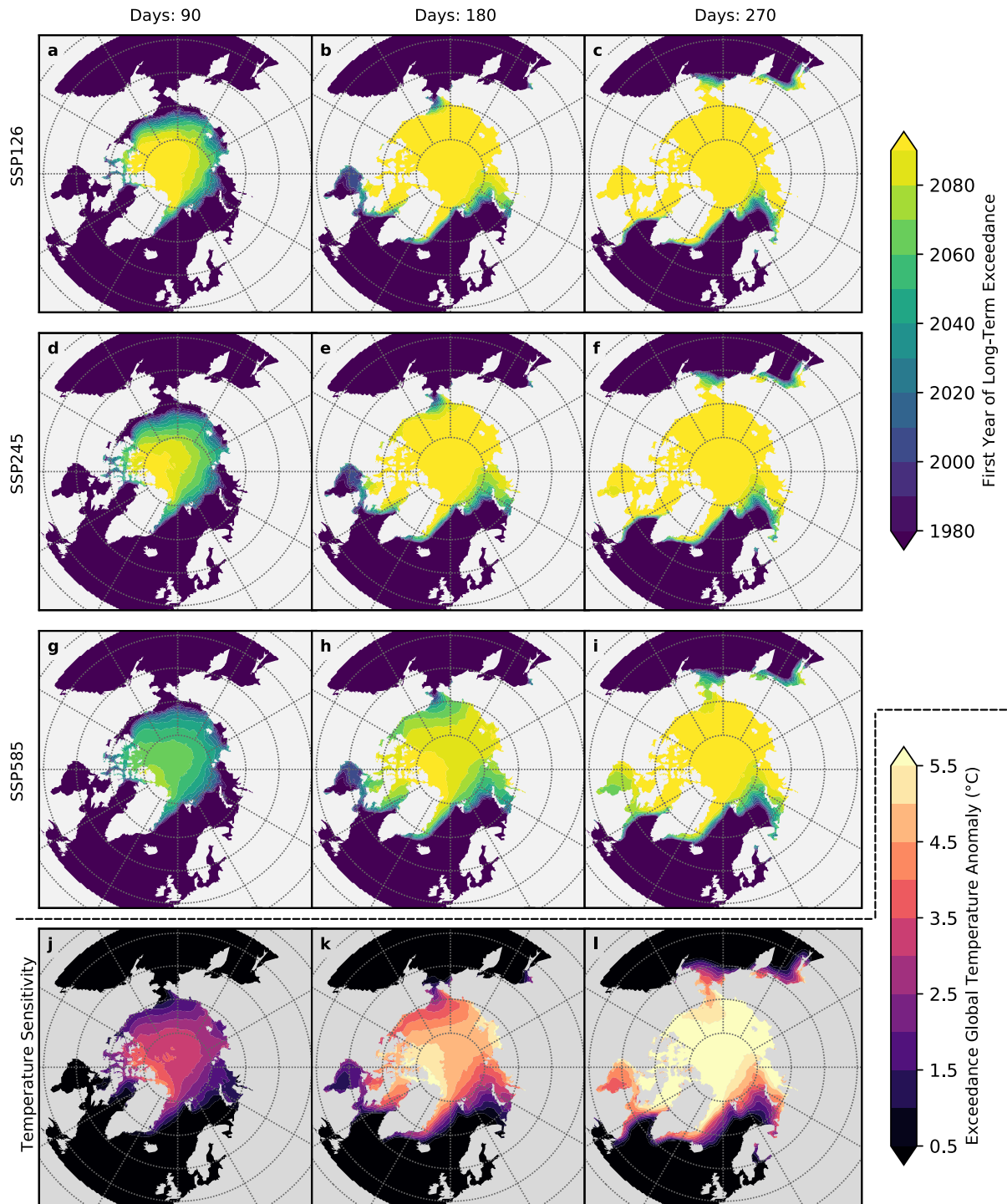


Fig. 4 Time and temperature when open-water period exceeds several thresholds. The year (a–i) and global temperature anomaly (j–l) at which the open-water period exceeds 90 days (left), 180 days (center), or 270 days (right) in the CMIP6 multi-model mean. Exceedance year is the first year for which the open-water period exceeds the threshold for the next 5 years. Temperature anomalies are with respect to 1850–1900 and use the SSP585 experiment.

show that trends toward later advance outpace trends toward earlier retreat in the future (Fig. 3). Under the strong warming scenario, the projected open-water period exceeds 6 months for most of the Arctic by the end of the century (Figs. 2 and 4). However, the magnitude of change varies greatly by region.

Beyond updating open-water period projections with CMIP6 models, this study refines our projections by assessing the sensitivity of open-water period (and sea ice retreat/advance) to

global temperature anomalies. This controls for bias models may have on warming rates^{40,41}. Moreover, warming rates dictate the rate of change for open-water period. For example, the timing of divergence in open-water period in the emissions scenarios (Fig. 2) aligns with the timing of divergence in global temperature (Supplementary Fig. 1). On average for the study area, an increase of 2°C from 1850–1900 increases the open-water period by 2 months (Fig. 3). At 1.5°C of warming, the increase is about

1.5 months (Supplementary Fig. 10). Regional assessments also refine our understanding. For example, the lengthening open-water period with 2 °C warming is greater for the Beaufort, Chukchi, East Siberian, and Kara Seas (3.0–3.5 months) and greatest for the Barents Sea (4 months).

The opening of the Transpolar Sea Route (SIC < 15%) for over 90 days with 3.5 °C of warming and over 180 days with 5.0 °C (Fig. 4) will benefit commercial shipping^{20,42}. Similar benefits to shipping will also occur in Hudson Bay and Hudson Strait^{15,20}, with over 180 days of open water with 1.5 °C of warming and over 270 days with 5.0 °C. However, benefits of a longer open water period will be countered by costs related to issues such as coastal erosion¹⁸ and disruption of hunting and fishing practices^{13,19}. For example, loss of winter sea ice in the Gulf of St. Lawrence will force northward migration of harp seals and hooded seals, which require pack ice for pupping^{43,44}. Most CMIP6 models project open water year-round in the Gulf of St. Lawrence with even 1.5 °C of warming. The dramatic increase of the open-water period in the Chukchi and Beaufort Seas will likewise lead to major disruptions of ecosystems and social systems, including for subsistence whaling^{45,46} and hunting of walrus⁴⁷. Many of the changes reported here will occur even if warming is limited to 2 °C. However, the most dramatic changes (e.g., opening of Transpolar Sea Route for 90 or 180 days) will only occur with greater levels of warming (e.g., 3.5 or 5.0 °C). If and when these larger changes occur depends on the future of global emissions.

Methods

Datasets. SIC and temperature data were downloaded^{48,49} from four CMIP6 experiments: historical, SSP126, SSP245, and SSP585. Monthly surface air temperature (“tas”) was downloaded for all models. For SIC, the “siconc” variable (on the ocean grid) was used when possible; “siconca” (on the atmospheric grid) was used for UKESM1-0-LL. Most of the analyses in this study involve spatial averaging, so regridding is unnecessary except for figures involving maps of the multi-model mean (e.g., Fig. 4). In those cases, bilinear interpolation to a Lambert Azimuthal Equal-Area grid is employed.

One model (CMCC-CM2-SR5) was removed from consideration because of excessively long open-water periods for the historical experiment (Supplementary Fig. 11). Detection of sea ice retreat and advance dates requires daily observations, so only models with daily output as of May 2020 were included. Additionally, only model simulations that had daily SIC for the period 1950–2014 (historical) and 2015–2100 (emissions scenarios) were included. In total, 21 models were used, ranging from 69 to 192 simulations, depending on the experiment (Supplementary Table 1). Six additional models (Supplementary Table 2) include daily SIC only for the historical experiment. Using all 27 models to assess bias (Supplementary Fig. 12) yields only minor differences compared to Fig. 1. Many CMIP6 model are submitted with multiple simulations, but the number of simulations differs. To provide equal weight to all models, the multi-model means are always calculated from the first simulation of each model (usually denoted as “realization 1” or “r1”).

To test for bias in CMIP6 models, results are compared to three observational sea ice data sets and four observational temperature records. Multiple observational datasets are used because of significant differences between products⁵⁰. Daily SIC for the period of overlap between the modern satellite record and historical CMIP6 simulations (1979–2014) was acquired from the Bootstrap^{51,52}, NASA-Team^{53,54}, and OSI SAF^{55,56} datasets. Linear interpolation through time is used to fill in missing days at the beginning of the record (1979–1987). The pole hole for NASA-Team and Bootstrap algorithms is filled using the average SIC in the ring of grid cells within 1° latitude of the pole hole edge. The OSI SAF product already has a filled pole hole. Monthly temperature observations for the historical period were obtained from Berkeley Earth (1850–2014)⁵⁷, GISTemp v4 (1880–2014)^{58,59}, HadCRUT4.6.0.0 (1850–2014)⁶⁰, and NOAA GlobalTemp v5 (1880–2014)^{61,62}.

Open-water period calculation. As in several past studies^{24,25,34} the open-water period for a given SIC threshold is defined as the continuous period between the last SIC observation above that threshold prior to the day of annual minimum SIC (hereafter “retreat day”) and the first SIC observation above that threshold after the annual minimum (hereafter “advance day”). The annual minimum day is defined as the median of all days August–October that equal the minimum SIC for the year. Having multiple days equal to the SIC minimum is most common for grid cells that have a long period of 0% SIC in summer. Following Stroeve et al.²⁴, a 5-day moving average is applied to the daily SIC time series at each grid cell prior to detection of the open-water period to reduce the impact of short-term SIC fluctuations.

The only modification from the Stroeve et al.²⁴ method is our definition of the sea ice year. Since Arctic sea ice reaches its maximum extent every March, most studies^{24,25,34} of sea ice retreat and advance in the Arctic identify sea ice retreat for a given year (e.g., 2001) as occurring sometime after March 1 (e.g., after March 1, 2001) and sea ice advance as occurring before March 1 of the following year (e.g., before March 1, 2002). In this study, we define the sea ice year as starting on the median of all days January–April for which SIC equals the maximum SIC for that period. A dynamic start day is employed because a common start and end day for each year (e.g., March 1) can lead to underestimation of open-water periods for grid cells at the edge of the winter sea ice pack²⁷. The retreat day always occurs between the maximum day and minimum day of the same year, and the advance day always occurs between the minimum day and the subsequent year’s maximum day. It is possible for individual years to have open-water periods in excess of 365 (or 366) days in grid cells at the fringes of the sea ice pack in winter; however, the average open-water period will approach a number less than or equal to 365 (or 365.25) days as the averaging period increases since each day can only be assigned to one open-water period.

The concept of “open-water period” can range from predominantly ice-covered with some open water (e.g., SIC = 80%) to nearly ice-free conditions (e.g., SIC = 15%). For example, Peng et al.⁶³ used the 15% and 80% SIC thresholds to define an “inner” and “outer” ice-free period, respectively. Smith et al.³⁴ also used 80% as the “outer ice-free period” but called 15% the “open period”. We highlight 15% here because of its frequent use^{30,31,64} and suitability for transit by open-water vessels⁶⁵. Results for 80% show longer open-water periods but similar biases, trends, and sensitivity to temperature (Supplementary Figs. 3–5).

Bias assessment. Comparison of historical simulations in CMIP6 to observations is based on the SIMIP Community¹¹ methodology. All multi-model means are calculated from the first simulation of each model. Uncertainty arising from internal variability (σ_{cmip6}) is calculated by taking the average standard deviation (σ_m ; Eq. 1) for all models with an ensemble of at least three simulations for the historical experiment. For each model m with n simulations, σ_m is calculated as the standard deviation (s ; Eq. 2) across all simulations adjusted by the scale mean of the chi distribution with $n - 1$ degrees of freedom ($c_4(n)$; Eq. 3), where x_i is the value for each simulation of that model, \bar{x}_m is the mean for that model’s ensemble, and Γ represents the gamma function.

$$\sigma_m = \frac{s}{c_4(n)} \quad (1)$$

$$s = \sqrt{\frac{\sum (x_i - \bar{x}_m)^2}{n - 1}} \quad (2)$$

$$c_4(n) = \sqrt{\frac{2}{n - 1} \frac{\Gamma(\frac{n}{2})}{\Gamma(\frac{n-1}{2})}} \quad (3)$$

An adjusted standard deviation is used because of the small sample size ($n \geq 3$). Observational uncertainty (σ_{obs}) is calculated as the range of all observational datasets. Plausible simulations are those within the range

$$\bar{x}_{\text{obs}} \pm 2\sqrt{\sigma_{\text{cmip6}}^2 + \sigma_{\text{obs}}^2} \quad (4)$$

where \bar{x}_{obs} and σ_{obs} are the mean and standard deviation of the observational datasets. Averages, trends, and temperature sensitivity are compared for the overlap period of 1979–2013. Because annual retreat and advance of sea ice requires several months from the subsequent year, a full open-water period cannot be computed for 2014 in the historical simulations or for 2100 in the emissions scenarios.

Comparing sea ice to temperature. Following the Intergovernmental Panel on Climate Change⁶⁶, the baseline period for calculating temperature anomalies is 1850–1900. All CMIP6 models have temperature data for this period; however, two of the observational temperature records (NOAA GlobalTemp and GISTemp) only go back to 1880. The linear relationship between the average of these two records and the average of the Berkeley Earth and HadCRUT records for the period 1880–2014 is used to extrapolate back to 1850. This decreases the 1850–1900 observational mean by 0.018 °C compared to using the Berkeley and HadCRUT records alone. Sea ice variables are computed for global temperature anomalies (e.g., 0 and 2 °C) using the sensitivity of each variable to temperature ($\Delta X/\Delta T$) for the given model and experiment.

Creating a time series of area-weighted spatial averages of the open-water period for 15 regions (defined in Supplementary Fig. 13) is straightforward. However, retreat day and advance day are invalid for years when SIC is always above or always below the SIC threshold. Past studies have variably assigned a default value to such cases⁶⁷, excluded grid cells that lack a clear retreat/advance cycle for a sufficient percentage of years^{23,30}, worked with grid-cell-specific anomalies instead⁶³, or examined histograms for each region rather than a regional average³⁴. For examining a long period of strong external forcing like 1850–2100, these methods may produce results that are biased by the changing spatial domain of seasonal sea ice. For example, if a grid cell has 300 days of open water in 1850,

but by 2100 it is permanently open water, that grid cell will have no valid retreat or advance day in 2100. If such grid cells are included in spatial averaging only when valid, or if non-valid years are filled with a constant value, trends may be biased as a result. If such grid cells are omitted from analysis, the study area shrinks to only grid cells that have a maximum SIC above 15% and a minimum SIC 15% in every year 1850–2100, which makes the study area vanishingly small for SSP585.

Therefore, we aggregate for retreat day by calculating the percentage of area in a region for which sea ice is either always below 15% or falls below 15% by a certain date. For advance, this is the percentage of area in a region for which sea ice is either never above 15% or rises above 15% after a certain date. This method is better for long-term analysis because the averaging domain never changes. For each region, benchmark dates were chosen as the closest first and last day of a month to the median retreat and advance day, respectively, for a SIC threshold of 50% during 1979–2013. This method minimizes cases with 0 or 100% of grid cells meeting the retreat or advance criteria for any region and any SIC threshold ranging from 15 to 80%.

Data availability

CMIP6 data were downloaded from <https://esgf-node.llnl.gov/search/cmip6/>. Bootstrap, NASA-Team, and OSI SAF sea ice data were downloaded from <https://nsidc.org/data/NSIDC-0079/versions/3>, <https://nsidc.org/data/NSIDC-0051/versions/1>, and <http://www.osi-saf.org/?q=content/global-sea-ice-concentration-climate-data-record-smrassmissmis>, respectively. Berkeley Earth, GISTemp v4, HadCRUT4.6.0.0, and NOAA GlobalTemp v5.0.0 temperature data were downloaded from <http://berkeleyearth.org/data-new/>, <https://data.giss.nasa.gov/gistemp/>, <https://www.metoffice.gov.uk/hadobs/hadcrut4/>, <https://www.nccei.noaa.gov/thredds/catalog/noaa-global-temp-v5/catalog.html>, respectively. Results derived from these data sources are available at <https://doi.org/10.6084/m9.figshare.14484816.v1> and <https://doi.org/10.6084/m9.figshare.14484762>.

Code availability

Python and R scripts used to process these datasets are available at <https://doi.org/10.5281/zenodo.4730450>. CMIP6 data were downloaded using version 1.2.0 of Thiago Loureiro's CMIP6 downloader (<https://doi.org/10.5281/zenodo.3966556>).

Received: 9 April 2021; Accepted: 10 May 2021;

Published online: 03 June 2021

References

- IPCC. Climate change 2001: the scientific basis. In *Contribution of Working Group I to the Third Assessment Report of the Intergovernmental Panel on Climate Change* (eds. Houghton et al.) 1–881 (Cambridge University Press, 2001).
- Meier, W. N., Stroeve, J. & Fetterer, F. Whither Arctic sea ice? A clear signal of decline regionally, seasonally and extending beyond the satellite record. *Ann. Glaciol.* **46**, 428–434 (2007).
- Stroeve, J. C. et al. The Arctic's rapidly shrinking sea ice cover: a research synthesis. *Clim. Change* **110**, 1005–1027 (2012).
- Onarheim, I. H., Eldevik, T., Smedsrud, L. H. & Stroeve, J. C. Seasonal and regional manifestation of Arctic sea ice loss. *J. Clim.* **31**, 4917–4932 (2018).
- Kwok, R. Arctic sea ice thickness, volume, and multiyear ice coverage: losses and coupled variability (1958–2018). *Env. Res. Lett.* **13**, 105005 (2018).
- Notz, D. & Stroeve, J. The trajectory towards a seasonally ice-free Arctic ocean. *Curr. Clim. Change Rep.* **4**, 407–416 (2018).
- Jahn, A. Reduced probability of ice-free summers for 1.5 °C compared to 2 °C warming. *Nat. Clim. Change* **8**, 409–413 (2018).
- Sigmond, M., Fyfe, J. C. & Swart, N. C. Ice-free Arctic projections under the Paris Agreement. *Nat. Clim. Change* **8**, 404–408 (2018).
- Wang, M. & Overland, J. E. A sea ice free summer Arctic within 30 years? *Geophys. Res. Lett.* **36**, L07502 (2009).
- Årthun, M., Onarheim, I. H., Dörr, J. & Eldevik, T. The seasonal and regional transition to an ice-free Arctic. *Geophys. Res. Lett.* **48**, e2020GL090825 (2021).
- Community, S. Arctic sea ice in CMIP6. *Geophys. Res. Lett.* **47**, e2019GL086749 (2020).
- Landrum, L. & Holland, M. M. Extremes become routine in an emerging new Arctic. *Nat. Clim. Change* **10**, 1108–1115 (2020).
- Laidler, G. J. et al. Travelling and hunting in a changing Arctic: assessing Inuit vulnerability to sea ice change in Igloodik, Nunavut. *Clim. Change* **94**, 363–397 (2008).
- Shibata, H., Izumiyama, K., Tateyama, K., Enomoto, H. & Takahashi, S. Sea-ice coverage variability on the Northern sea routes, 1980–2011. *Ann. Glaciol.* **54**, 139–148 (2013).
- Andrews, J., Babb, D. & Barber, D. G. Climate change and sea ice: shipping in Hudson Bay, Hudson Strait, and Foxe Basin (1980–2016). *Elementa Sci. Anthropol.* **6**, 19 (2018).
- Kahru, M., Manzano-Sarabina, M. & Mitchell, B. G. Are phytoplankton blooms occurring earlier in the Arctic. *Glob. Change Biol.* **17**, 1733–1739 (2011).
- Arrigo, K. R. & Dijken, G. Lvan Continued increases in Arctic Ocean primary production. *Prog. Oceanogr.* **136**, 60–70 (2015).
- Overeem, I. et al. Sea ice loss enhances wave action at the Arctic coast. *Geophys. Res. Lett.* **38**, L17503 (2011).
- Galappaththi, E. K., Ford, J. D., Bennett, E. M. & Berkes, F. Climate change and community fisheries in the arctic: a case study from Pangnirtung, Canada. *J. Env. Manage.* **250**, L109534 (2019).
- Wagner, P. M. et al. Sea-ice information and forecast needs for industry maritime stakeholders. *Polar Geogr.* **43**, 160–187 (2020).
- Simmonds, I. & Rudeva, I. A comparison of tracking methods for extreme cyclones in the Arctic basin. *Tellus A* **66**, 25252 (2014).
- Stammerjohn, S., Massom, R., Rind, D. & Martinson, D. Regions of rapid sea ice change: an inter-hemispheric seasonal comparison. *Geophys. Res. Lett.* **39**, L06501 (2012).
- Collow, T. W., Wang, W., Kumar, A. & Zhang, J. How well can the observed Arctic sea ice summer retreat and winter advance be represented in the NCEP Climate Forecast System version 2? *Clim. Dyn.* **49**, 1651–1663 (2016).
- Stroeve, J. C., Crawford, A. D. & Stammerjohn, S. Using timing of ice retreat to predict timing of fall freeze-up in the Arctic. *Geophys. Res. Lett.* **43**, 6332–6340 (2016).
- Bliss, A. C., Steele, M., Peng, G., Meier, W. N. & Dickinson, S. Regional variability of Arctic sea ice seasonal change climate indicators from a passive microwave climate data record. *Env. Res. Lett.* **14**, 045003 (2019).
- Serzeze, M. C., Crawford, A. D., Stroeve, J. C., Barrett, A. P. & Woodgate, R. A. Variability, trends, and predictability of seasonal sea ice retreat and advance in the Chukchi Sea. *J. Geophys. Res. Oceans* **127**, 7308–7325 (2016).
- Wang, M., Yang, Q., Overland, J. E. & Stabenro, P. Sea-ice cover timing in the Pacific Arctic: the present and projections to mid-century by selected CMIP5 models. *Deep Sea Res. Pt II* **152**, 22–34 (2018).
- Timmermans, M. L. The impact of stored solar heat on Arctic sea ice growth. *Geophys. Res. Lett.* **42**, 6399–6406 (2015).
- Steele, M. & Dickinson, S. The phenology of Arctic Ocean surface warming. *J. Geophys. Res. Oceans* **121**, 6847–6861 (2016).
- Lebrun, M., Vancoppenolle, M., Madec, G. & Massonnet, F. Arctic sea-ice-free season projected to extend into autumn. *Cryosphere* **13**, 79–96 (2019).
- Barnhart, K. R., Miller, C. R., Overeem, I. & Kay, J. E. Mapping the future expansion of Arctic open water. *Nat. Clim. Change* **6**, 280–285 (2015).
- Collins, M. et al. *Long-term Climate Change: Projections, Commitments and Irreversibility* (eds. Stocker, T. F. et al.) 1–108 (Cambridge University Press, 2013).
- Conference of the Parties, Adoption of the Paris Agreement, United Nations Doc. FCCC/CP/2015/L.9/Rev/1 (12 Dec. 2015).
- Smith, A., Jahn, A. & Wang, M. Seasonal transition dates can reveal biases in Arctic sea ice simulations. *Cryosphere* **14**, 2977–2997 (2020).
- Winton, M. Do climate models underestimate the sensitivity of Northern Hemisphere sea ice cover? *J. Clim.* **24**, 3924–3934 (2011).
- Rosenblum, E. & Eisenman, I. Sea ice trends in climate models only accurate in runs with biased global warming. *J. Clim.* **30**, 6265–6278 (2017).
- Perovich, D. K. et al. Increasing solar heating of the Arctic Ocean and adjacent seas, 1979–2005: attribution and role in the ice-albedo feedback. *Geophys. Res. Lett.* **34**, L19505 (2007).
- Kay, J. E. et al. The Community Earth System Model (CESM) large ensemble project: a community resource for studying climate change in the presence of internal climate variability. *Bull. Am. Meteorol. Soc.* **96**, 1333–1349 (2015).
- England, M., Jahn, A. & Polvani, L. Nonuniform contribution of internal variability to recent Arctic sea ice loss. *J. Clim.* **32**, 4039–4053 (2019).
- Mahlstein, I. & Knutti, R. September Arctic sea ice predicted to disappear near 2 °C global warming above present. *J. Geophys. Res.* **117**, D06104 (2012).
- Niederdröck, A. L. & Notz, D. Arctic sea ice in a 1.5 °C warmer world. *Geophys. Res. Lett.* **45**, 1963–1971 (2018).
- Laliberté, F., Howell, S. E. L. & Kushner, P. J. Regional variability of a projected sea ice-free Arctic during the summer months. *Geophys. Res. Lett.* **43**, 256–263 (2016).
- Johnston, D., Friedlaender, A., Torres, L. & Lavigne, D. Variation in sea ice cover on the east coast of Canada from 1969 to 2002: climate variability and implications for harp and hooded seals. *Clim. Res.* **29**, 209–222 (2005).
- Stenson, G. B. & Hammill, M. O. Can ice breeding seals adapt to habitat loss in a time of climate change? *ICES J. Mar. Sci.* **71**, 1977–1986 (2014).
- Ashjian, C. J. et al. Climate variability, oceanography, Bowhead whale distribution, and Inūpiat subsistence whaling near Barrow, Alaska. *Arctic* **63**, 179–194 (2010).
- Clarke, J. T., Kennedy, A. S. & Ferguson, M. C. Bowhead and gray Whale distributions, sighting rates, and habitat associations in the Eastern Chukchi Sea, Summer and Fall 2009–15, with a retrospective comparison to 1982–91. *Arctic* **69**, 359–377 (2016).

47. Jay, C., Fischbach, A. & Kochnev, A. Walrus areas of use in the Chukchi Sea during sparse sea ice cover. *Mar. Ecol. Prog. Ser.* **468**, 1–13 (2012).
48. Eyring, V. et al. Overview of the Coupled Model Intercomparison Project Phase 6 (CMIP6) experimental design and organisation. *Geosci. Model Dev. Discuss.* **8**, 10539–10583 (2015).
49. ESGF. The Earth System Grid Federation: an open infrastructure for access to distributed geospatial data. *Future Gener. Comput. Syst.* **36**, 400–417 (2014).
50. Meier, W. N. & Stewart, J. S. Assessing uncertainties in sea ice extent climate indicators. *Env. Res. Lett.* **14**, 035005 (2019).
51. Comiso, J. C., Cavalieri, D. J., Parkinson, C. L. & Gloersen, P. Passive microwave algorithms for sea ice concentration: a comparison of two techniques. *Remote Sens. Environ.* **60**, 357–384 (1997).
52. Comiso, J. C. *Bootstrap Sea Ice Concentrations from Nimbus-7 SMMR and DMSP SSM/I-SSMIS Version 3* (NASA National Snow and Ice Data Center, 2017).
53. Cavalieri, D. J., Parkinson, C. L., Gloersen, P. & Zwally, H. *Sea Ice Concentrations from Nimbus-7 SMMR and DMSP SSM/I-SSMIS Passive Microwave Data, Version 1* (NASA National Snow and Ice Data Center, 1996).
54. Markus, T. & Cavalieri, D. J. An enhancement of the NASA Team sea ice algorithm. *IEEE Trans. Geosci. Remote Sens.* **38**, 1387–1398 (2000).
55. OSI SAF. *Global Sea Ice Concentration Climate Data Record v2.0—Multimission, EUMETSAT SAF on Ocean and Sea Ice* (EUMETSAT Data Center, 2017).
56. Lavergne, T. et al. Version 2 of the EUMETSAT OSI SAF and ESA CCI sea-ice concentration climate data records. *Cryosphere* **13**, 49–78 (2019).
57. Rohde, R., Muller, R., Jacobsen, R., Perlmutter, S. & Mosher, S. Berkeley earth temperature averaging process. *Geoinformatics Geostatist.* **1**, <https://doi.org/10.4172/2327-4581.1000103> (2013).
58. Lenssen, N. J. L. et al. Improvements in the GISTEMP uncertainty model. *J. Geophys. Res. Atmos.* **124**, 6307–6326 (2019).
59. GISTEMP Team. *GISS Surface Temperature Analysis (GISTEMP)*, version 4 (NASA Goddard Institute for Space Studies, 2020).
60. Morice, C. P., Kennedy, J. J., Rayner, N. A. & Jones, P. D. Quantifying uncertainties in global and regional temperature change using an ensemble of observational estimates: The HadCRUT4 data set. *J. Geophys. Res.* **117**, D08101 (2012).
61. Vose, R. S. et al. NOAA’s merged land–ocean surface temperature analysis. *Bull. Am. Meteorol. Soc.* **93**, 1677–1685 (2012).
62. Zhang, H.-M., Huang, J., Lawrimore, J. H., Menne, M. J. & Smith, T. M. *NOAA Global Surface Temperature Dataset (NOAAGlobalTemp)*, Version 5.0. (NOAA National Centers for Environmental Information, 2019).
63. Peng, G., Steele, M., Bliss, A., Meier, W. & Dickinson, S. Temporal means and variability of Arctic sea ice melt and freeze season climate indicators using a satellite climate data record. *Remote Sens.* **10**, 1328–21 (2018).
64. Frey, K. E., Moore, G. W. K., Cooper, L. W. & Grebmeier, J. M. Divergent patterns of recent sea ice cover across the Bering, Chukchi, and Beaufort seas of the Pacific Arctic Region. *Prog. Oceanogr.* **136**, 32–49 (2015).
65. Lei, R. et al. Changes in sea ice conditions along the Arctic Northeast Passage from 1979 to 2012. *Cold Reg. Sci. Technol.* **119**, 132–144 (2015).
66. IPCC. in *Global Warming at 1.5 °C* (eds. Masson-Delmotte, V. P. et al.) (World Meteorological Organization, 2018).
67. Stammerjohn, S. E., Martinson, D. G., Smith, R. C., Yuan, X. & Rind, D. Trends in Antarctic annual sea ice retreat and advance and their relation to El Niño–Southern Oscillation and Southern Annular Mode variability. *J. Geophys. Res. Atmos.* **113**, C03S90 (2008).

Acknowledgements

J.S. and A.C. acknowledge funding support from the Canada Research Chairs Program (Canada 150) and NSERC RGPIN-2020-05689. A.S. acknowledges support from the Future Investigators in NASA Earth and Space Science and Technology Grant 80NSSC19K1324 and the NSF Graduate Research Fellowship (grant no. DGE 1144083). A.J. acknowledges support from NSF-award 1847398. This research supports the Climate and Cryosphere (CliC) endorsed CMIP6 diagnostic sea ice model intercomparison project (SIMIP: <http://www.climate-cryosphere.org/mips/simip>).

Author contributions

A.C. acquired and processed data, created figures, and led manuscript writing. J.S. led conceptualization of research questions. A.C., J.S., A.S., and A.J. contributed to forming the research plan, interpreting results, and writing the manuscript.

Competing interests

The authors declare no competing interests.

Additional information

Supplementary information The online version contains supplementary material available at <https://doi.org/10.1038/s43247-021-00183-x>.

Correspondence and requests for materials should be addressed to A.C.

Peer review information Primary handling editor: Heike Langenberg.

Reprints and permission information is available at <http://www.nature.com/reprints>

Publisher’s note Springer Nature remains neutral with regard to jurisdictional claims in published maps and institutional affiliations.



Open Access This article is licensed under a Creative Commons Attribution 4.0 International License, which permits use, sharing, adaptation, distribution and reproduction in any medium or format, as long as you give appropriate credit to the original author(s) and the source, provide a link to the Creative Commons license, and indicate if changes were made. The images or other third party material in this article are included in the article’s Creative Commons license, unless indicated otherwise in a credit line to the material. If material is not included in the article’s Creative Commons license and your intended use is not permitted by statutory regulation or exceeds the permitted use, you will need to obtain permission directly from the copyright holder. To view a copy of this license, visit <http://creativecommons.org/licenses/by/4.0/>.

© The Author(s) 2021